On analytical calculations of offshore fresh groundwater:

Influence of aquitard salinity structure

Silvia Cristina Solórzano Rivas

A research project submitted as a requirement for admission to the degree

of MASTER OF SCIENCE (GROUNDWATER HYDROLOGY)

FACULTY OF SCIENCE AND ENGINEERING

SCHOOL OF THE ENVIRONMENT

26 May 2017

Contents

List of Figures

List of Tables

Summary

Subsea freshwater is widespread around the globe, and is particularly dependent on the properties of offshore aquitards, which inhibit seawater-freshwater mixing and allow offshore freshwater to persist. However, little is known of the salinity structure in subsea aquitards, especially in relation to the offshore freshwater distribution. This is critical for the application of recent analytical solutions to subsea freshwater extent given requisite assumptions about aquitard salinity. In this research, numerical simulation of simplified conditions has been used to explore the extent of offshore freshwater in subsea aquifers and overlying aquitards, including in relation to the upward leakage of freshwater. The results show that available analytical solutions significantly overestimate the offshore extent of upwelling freshwater due to the presumption of seawater in the aquitard, whereas the seawater wedge toe is less sensitive to the assumed aquitard salinity. The use of implicit, conductance-based representations of the aquitard were also explored (i.e., using the popular SEAWAT code), finding that SEAWAT's implicit approach can represent the offshore distance of upwelling freshwater through modified parameterisation of the aquitard. The results show that an estimate of the upward freshwater flow that is required to freshen the aquitard is associated with the dimensionless Rayleigh number, whereby the critical Rayleigh number that distinguishes fresh and saline regions (based on the position of the 0.5 isochlor) within the aquitard is approximately two.

Declaration

I certify that this thesis does not incorporate without acknowledgment any material previously submitted for a degree or diploma in any university; and that to the best of my knowledge and belief it does not contain any material previously published or written by another person except where due reference is made in the text.

Signed..
Silvia Cristina Solorzano Rivas

Date....26 May 2017 ....

Acknowledgements

I would like to express my eternal gratitude to my supervisor, Professor Adrian Werner, this piece of research is product of his enthusiasm, guidance and wisdom, his constant encouraging words have made me love research. I also wish to thank Dr. Tariq Laattoe for introducing me to Python, this has been a very useful tool. Thank you for your willingness to help me. My husband, Javier, deserves special mention, since without his love, help and support, this Master degree could not have been accomplished. I cannot thank you enough. To my parents, who have always believed in me. And lastly, but the most important, I thank God, I could not have done this without His blessing.

1. Introduction

Despite the widespread presence of freshwater beneath the seafloor (e.g., Post et al., 2013) the processes accompanying the occurrence of fresh offshore groundwater are under-studied relative to the current knowledge of seawater-freshwater relationships in onshore aquifers. Case studies of freshwater bodies in offshore aquifers have been undertaken for Hong Kong (China) (Jiao et al., 2015; Kwong & Jiao, 2016); Suriname (Groen et al., 2000), and the Atlantic continental shelf (USA), including Nantucket Island (Marksamer et al., 2007) and the subsea aquifers near the border between Georgia and Florida (Johnston, 1983). In each of these cases, fresh offshore groundwater underlies an extensive low-permeability sequence (i.e., an aquitard), which inhibits mixing between the fresh groundwater and overlying seawater.

These offshore freshwater bodies may be the consequence of entrapped paleo-freshwater during the low sea levels at the Pleistocene epoch and/or derived from modern discharge originating from onshore aquifers (Cohen et al., 2010). Here, 'modern' discharge is defined as occurring under current sea levels, whereby favourable conditions lead to fresh discharge into offshore aquifers that creates offshore freshwater extending considerable seaward distances within continental shelves. Bakker (2006) studied such a system near the Georgia-Florida border (USA), where pre-development groundwater heads are thought to have created a fresh groundwater body that reaches the edge of the continental shelf (i.e., 120 km offshore). Kooi and Groen (2001) studied the size of hypothetical offshore freshwater reserves driven by propitious onshore groundwater conditions, also concluding that freshwater may extend tens of kilometres offshore as a result of modern groundwater discharge. In the remainder of this text, only the case of offshore fresh groundwater that is in equilibrium with the onshore conditions is considered, i.e., paleo-freshwater in offshore aquifers is neglected. According to Post et al. (2013), paleo-freshwater is an important worldwide phenomenon that can be regarded as a potential freshwater resource; however, in the interests of scrutinising the solution of Bakker (2006) (described later), paleo-freshwater is neglected. Figure 1-1 presents a schematic of the conceptual model.

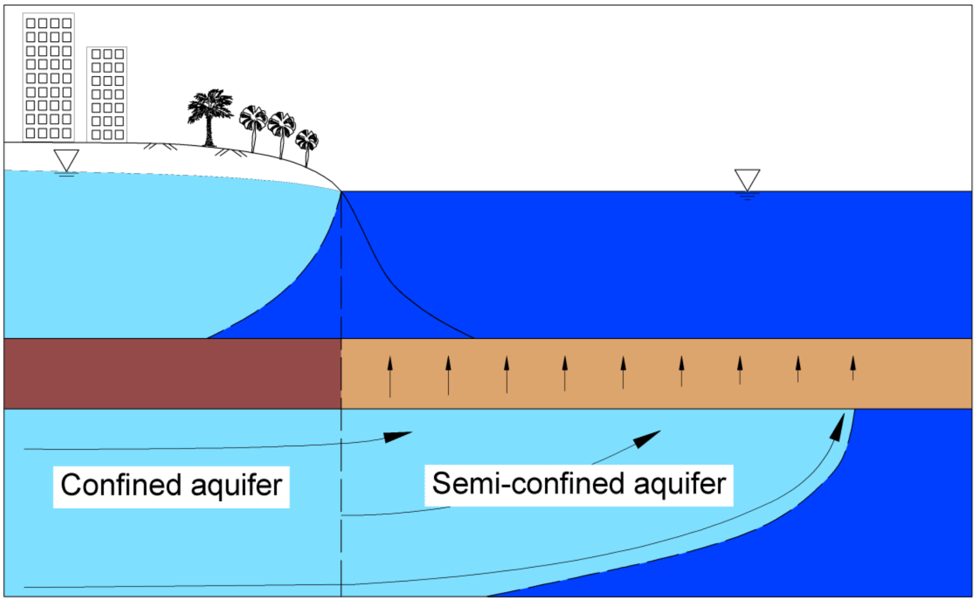

Figure 1-1. Conceptual model of a coastal aquifer-aquitard system with offshore extension, showing a typical freshwater-seawater distribution. Light blue is freshwater, and dark blue is seawater. The transition between freshwater and seawater is normally dispersive, but is drawn as a sharp interface for simplicity. Dark brown represents the impervious confining layer overlying the onshore aquifer, and light brown is the offshore aquitard, with upward leakage indicated by vertical arrows. Confined and semi-confined aquifers are underlain by an impervious basement.

Aside from the onshore hydraulic heads, other factors play critical roles in the offshore distribution of freshwater. For example, Frind (1982) concluded that the vertical hydraulic conductivity (K_z) of the subsea aquitard has a critical influence on the offshore distance of upward freshwater discharge, which in turn affects the salinity distribution in the underlying aquifer. He used two different values for K_z to demonstrate that the lower value resulted in increased thickness of the freshwater-seawater mixing zone and a larger offshore distance of freshwater leakage to the sea. Lu et al. (2013) undertook a more detailed analysis of the effect of K_z on freshwater-seawater mixing, and showed that as the aquitard-aquifer contrast in hydraulic conductivity increases, refraction across the aquitard-aquifer interface creates a broader mixing zone in the aquitard.

Analytical solutions to the steady-state extent of freshwater under the sea in offshore semi-confined aquifers have been produced by Edelman (1972), Kooi and Groen (2001), and Bakker (2006). They adopted steady-state, sharp-interface representations of the freshwater-seawater mixing zone and other simplifications to enable mathematical tractability. In these solutions, fresh groundwater discharge through the overlying subsea aquitard is treated as a head-dependent leakage term. This calculation requires that the groundwater salinity within the aquitard is a-priori known. In the analytical solutions of Kooi and Groen (2001) and Bakker (2006), the entire offshore aquitard is presumed to contain seawater. The implications of this assumption, in terms of the predictability of these analytical approaches, is the focus of the current analysis. The upward leakage of freshwater in Bakker's (2006) solution is expected to create freshening of the overlying aquitard, as opposed to it containing seawater. This is scrutinised by considering advective, dispersive and buoyancy forces occurring within the aquitard, i.e., due to seawater above the aquitard and freshwater below it.

The primary aim of this study is to assess the offshore extent of freshwater and seawater in both the aquifer and aquitard below the sea in idealised coastal aquifer settings, i.e., under conditions that allow for comparison with the Bakker (2006) solution. The salinity distributions in subsea aquitards are explored in relation to subsea freshwater extent and the accompanying upward leakage of freshwater to the sea, using numerical models. In applying the popular SEAWAT code to reproduce numerically Bakker's (2006) analytical solution, attempts to model the offshore aquitard using an implicit representation (i.e., a head-dependent boundary condition), as an approximation of the explicit representation of the aquitard are also presented. While the implicit method is numerically efficient, it has not been evaluated with respect to the more physically reliable explicit approach, in terms of subsea aquifer-aquitard simulation. Both explicit and implicit models are used to explore the assumptions adopted by Bakker (2006) regarding the aquitard salinity.

2. Methodology

2.1 Analytical Solution

Edelman (1972) developed the first analytical solution of the extent of offshore freshwater within a semi-confined subsea aquifer, where buoyancy forces and the location of the freshwater-seawater interface influence the upwelling freshwater discharge through the offshore aquitard. In his solution, the tip of the interface (i.e., where the interface intersects the top of the aquifer) is offshore and the freshwater body otherwise occurs as a lens, similar to the situation of small islands. Kooi and Groen (2001) produced a solution for the situation when the toe (i.e., where the interface intersects the bottom of the aquifer) is offshore. Both Edelman (1972) and Kooi and Groen (2001) considered infinitely long offshore aquifer-aquitard systems. Bakker (2006) built on their solutions by solving for the situation where freshwater reaches the offshore limit of the subsea aquifer (i.e., the edge of the continental shelf), which he represented as a vertical boundary that reflects the hydrostatic head of the sea. Bakker's (2006) conceptual model is consistent with the situation illustrated in Figure 1-1; an offshore semi-confined aquifer containing freshwater and seawater that are in equilibrium (i.e., steady-state conditions), and connected to a confined onshore aquifer. Freshwater enters the aquifer at the landward boundary, and eventually flows above a body of seawater, assumed immobile. The shape of the freshwater-seawater interface, which is treated as a sharp, pressure-equilibrium boundary, is a function of buoyancy forces arising from the density difference between freshwater and seawater. Losses of freshwater from the offshore aquifer, referred to here as submarine fresh groundwater discharge (SFGD), occur as upward seepage through the offshore aquitard, or as outflow where the aquifer is exposed at the continental shelf. Figure 1-1 illustrates the case where offshore freshwater does not extend to the continental shelf, and therefore the only discharge pathway for SFGD from the semi-confined aquifer is via upward leakage through the aquitard.

Figure 2-1 shows the 2D cross section and associated variables adopted by Bakker (2006) in developing his analytical solution. The onshore confined aquifer and offshore semi-confined aquifer have uniform thickness (*H*), and are assumed horizontal, homogeneous and isotropic. The offshore aquitard has a uniform thickness (H_l), and is overlain by a depth of seawater equal to H_s. The offshore domain extends a distance L_s to the continental shelf, which is represented by a vertical, specified-head boundary condition of hydrostatic seawater heads. Freshwater inflow (Q_c) [L^2 T^{-1}] to the model domain occurs through the left-hand boundary, which is situated at L_c from the shoreline. The sea level is z_s above the base of the aquifer. Freshwater and seawater densities are designated ρ_f and ρ_s, respectively.

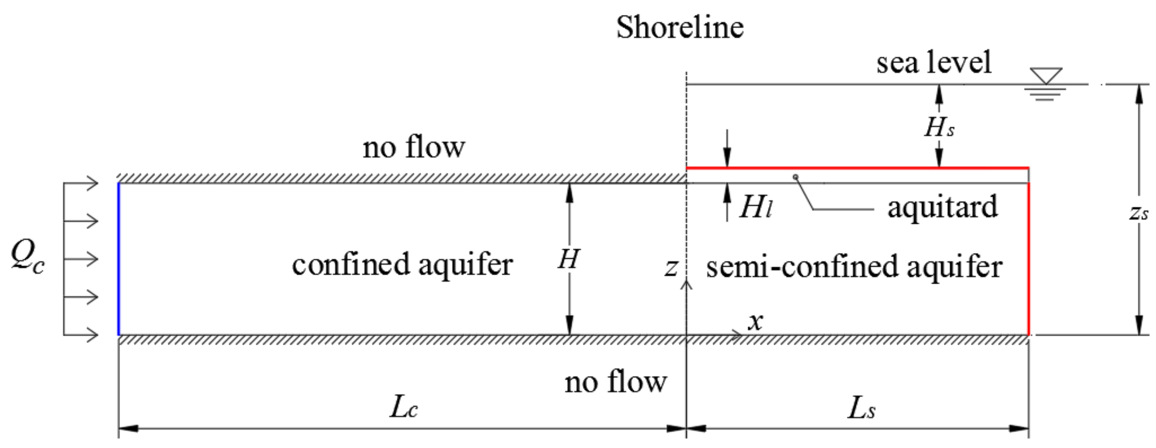

Figure 2-1. Conceptual model of a confined onshore aquifer with semi-confined offshore extension. Colour lines represent the salinity (blue = freshwater, red = seawater) of water entering the domain through boundaries. No-flow boundary conditions are used above and below the confined aquifer, and below the semi-confined aquifer.

The equivalent freshwater head of the sea at the top of the aquitard (h_t) is given by (Bakker, 2006):

$$h_t = z_s + \frac{\rho_s - \rho_f}{\rho_f} H_s \tag{1}$$

Application of Darcy's law, accounting for the buoyancy force that arises from the assumption of seawater in the aquitard, produces the following equation for upward freshwater flow (q_z) [L T^{-1}].

$$q_z = K_z \left(\frac{h - h_t}{H_l} - \frac{\rho_s - \rho_f}{\rho_f} \right) \tag{2}$$

Here, h is the head within the freshwater region of the subsea aquifer, and K_z is the vertical hydraulic conductivity, in this case of the aquitard [L T^{-1}]. If the aquitard contains freshwater, the buoyancy term, $(\rho_s - \rho_f)/\rho_f$, should be removed from equation (2). Bakker (2006) rewrites equation (2) in terms of the equivalent freshwater head of the sea at the base of the aquitard (h_s), defined in terms of h_t as:

$$h_s = h_t + \frac{\rho_s - \rho_f}{\rho_f} H_l \tag{3}$$

Combining equations (2) and (3) produces (Bakker, 2006):

$$q_z = \frac{K_z}{H_l} \left(h - h_s \right) \tag{4}$$

Bakker (2006) identifies four possible situations (Figure 2-2) regarding the position of the interface toe and tip relative to both the shoreline and continental shelf boundary. In this regard, Case I and Case II present an interface tip intersecting the top of the offshore semi-confined aquifer, or bottom of the aquitard, and therefore, the length of the aquitard is considered so large that the total freshwater discharge occurs through the leaky layer before the interface flow reaches the end of the aquitard (Bakker, 2006). However, for Case I, the interface toe reaches the confined section of the aquifer, that is, the toe is onshore, whereas for Case II, the interface is completely developed in the offshore, or semi-confined section. Similarly, for Cases III and IV, the interface toes reach the onshore and offshore sections respectively while the length of the aquitard is so short that the leakage zone occurs along the total length, and therefore is assumed that the interface reaches the vertical outflow face, that is, the end of the semi-confined section (Bakker, 2006).

Which of the four cases arises from a particular set of parameters is determined using two dimensionless parameters. These then lead to relevant analytical solutions to solve for the extent of offshore freshwater. Bakker et al. (2017) correct an inaccuracy in Bakker (2006) regarding the evaluation of the incomplete elliptic integrals for the solution of the two cases where the tip of the interface reaches the edge of the continental shelf (i.e., Cases III and IV).

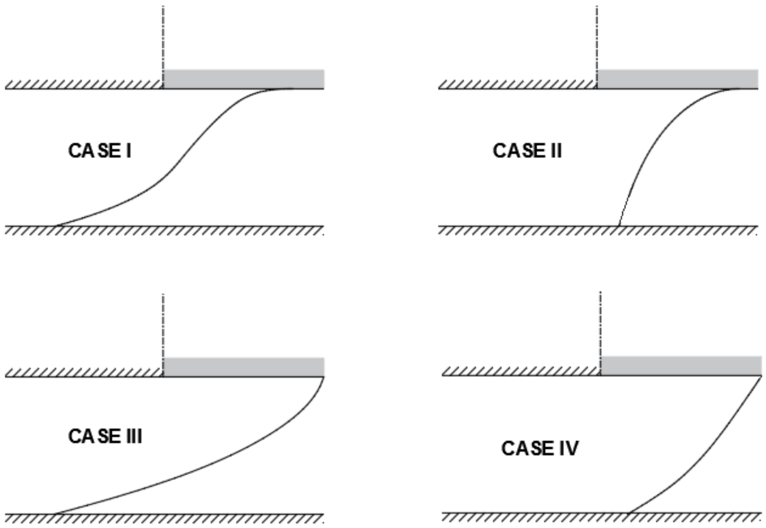

Figure 2-2. Four cases of interface position, modified from Bakker (2006)

To calculate the interface location arising from Bakker's (2006) method, the inland specified-flux boundary condition was replaced with a specified-head condition because inland head values are preferred as input to the problem. The head boundary condition was satisfied using a numerical shooting approach based on the classical 4th-order Runge-Kutta technique (Thomann, 2017). This approach was necessary because the head-based method provided by Bakker et al. (2017) was not available at the time of our investigation

2.2 Mixed-convection analysis

The situation of offshore freshwater is an unstable density configuration, where higher-density seawater overlies lower-density freshwater. That is, buoyancy (or gravity) forces tend to act downwards on the seawater where it overlies freshwater. In the conceptual model illustrated in Figure 1-1, freshwater moves upwards through the aquitard, escaping from the subsea aquifer, and thus, the salinity in the aquitard is a function of mixed convective processes (Simmons et al., 2010). That is, upward freshwater flow (advection) driven by head gradients is opposed by buoyancy forces arising from the freshwater-seawater density difference. Wooding et al. (1997) attempted to predict the salinity distribution within low-permeable sediments subject to mixed-convective processes. In their case, the density gradient is formed by evaporative concentration at the surface of a salt lake (Figure 2-3). They showed that the solute motion in unstable density configurations is initially driven by solute dispersion, which forms a saline boundary layer. If the upward flow of freshwater is sufficient to counteract dispersion, the conditions may remain in equilibrium thereby avoiding the creation of density-driven solute fingers. Wooding et al. (1997) considered dispersion as only molecular diffusion, and neglected mechanical dispersion in boundary layer development.

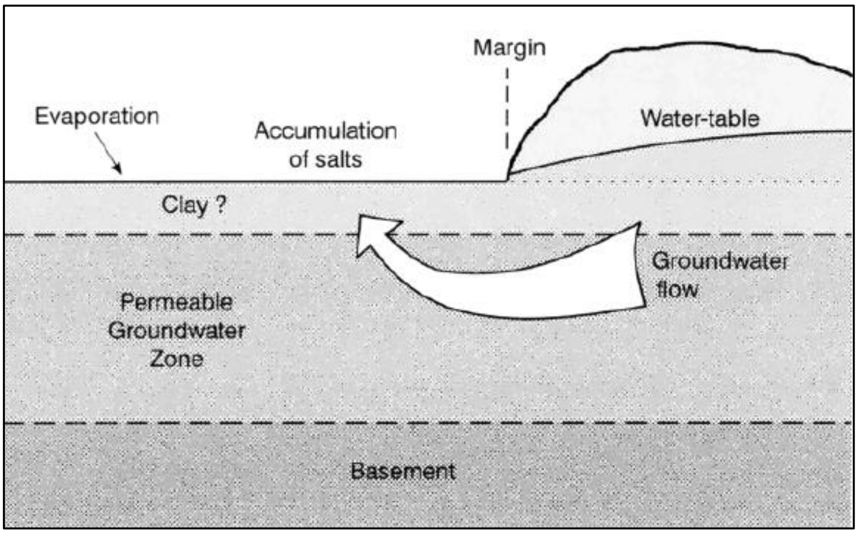

Figure 2-3. Conceptual model used by Wooding et al. (1997) in their onset analysis of density-driven flow beneath an evaporating salt lake.

Based on these principles and under equilibrium conditions, Kooi and Groen (2001) simplified the saline boundary layer thickness (δ) to:

$$\delta = \frac{D_m}{q_z} \quad (5)$$

Here, q_z is the Darcy velocity of vertical freshwater flow [L T^{-1}] and D_m is molecular diffusion [L^2 T^{-1}].

The onset of instability in the boundary layer, that is, when free convective forces overcome diffusion and dispersion, is given by the boundary Rayleigh number (Wooding et al., 1997):

$$Ra_\delta = \frac{(\rho_s - \rho_f)K_z\delta}{\rho_f D_m} \quad (6)$$

The Rayleigh number is a dimensionless parameter defined by the ratio between density-driven forces (i.e., buoyancy) and resistive forces (i.e., dispersion) (Simmons et al., 2010). A critical value of the Rayleigh number (Ra_c) exists whereby diffusive transport transitions to convective transport. Wooding et al. (1997) found that Ra_c is approximately 10 in silty and sandy clay-bearing sediments. That is, convective flow will occur in the form of unstable fingers in the boundary layer once Ra_δ exceeds 10. On this basis, Kooi and Groen (2001) suggested that complete salinization of the aquitard will occur when the aquitard thickness is equal to δ. They then used this definition to redefine the location of the seawater tip, whereby their analytical estimate of the offshore freshwater length was modified such that SFGD is terminated at the offshore position where δ equals H_l. Although they do not report values of Ra_δ, the approach adopted by Kooi and Groen (2001) resulted in a reduction of 50-80% of the offshore freshwater length for the various cases that were analysed. Unfortunately, they were unable to obtain consistent agreement between their numerical simulations and their δ-based truncation of the offshore freshwater extent. In the subsequent analytical development provided by Bakker (2006), there is no consideration of boundary layer development and the possibility that it truncates the extent of offshore SFGD.

Smith and Turner (2001) used a modified form of the Rayleigh number (Ra^*) to analyse the effects of mixed convection within a two-dimensional cross-sectional model of freshwater discharge to a saline esturay. Their conceptual model bears many similarities to the current one, except the estuary was represented as a horizontal, one-dimensional boundary condition (i.e., non-penetrating and immediately overlying the aquifer) of specified head and concentration. That is, the intervening aquitard considered in Figures 1-1 and 2-1 was not included. They proposed the following Rayleigh number formulation:

$$Ra^* = \frac{KH}{n_e U_d \alpha_L}\left(\frac{\rho_s - \rho_f}{\rho_f}\right) \times \frac{U_+}{U_-} \qquad (7)$$

Here, K is the aquifer's (isotropic) hydraulic conductivity [L T^{-1}], n_e is the effective porosity [-], U_d represents the average regional freshwater discharge velocity across the 1D estuary boundary (which represents the aquitard in the present study) [L T^{-1}], given by $q_c\, H/L_{0.5}$, where q_c is Q_c/H assuming unit cell width perpendicular to the cross section [L T^{-1}], and $L_{0.5}$ is the length of upward flow up to the 0.5 isochlor [L], α_L is the longitudinal dispersivity [L], and U_+/U_- is the regional discharge ratio between the flow crossing the left-hand and right-hand boundaries, respectively. Application of equation (7) to the Figure 1-1 requires that U_+/U_- is one, so that the problem is treated as symmetric. From numerical experimentation, Smith and Turner (2001) concluded that the critical Ra^* (Ra^*_c) for the occurrence of saltwater below the estuary is approximately five.

The three applications of Rayleigh theory described above (i.e., Wooding et al., 1997; Smith and Turner, 2001; Kooi and Groen, 2001) differ to the current situation. For example, while Wooding et al. (1997) consider mixed-convective forces in a vertical, homogeneous, one-dimensionless setting, the problem analysed here contains two materials (aquifer and aquitard) in a two-dimensional flow field. Smith and Turner's (2001) saltwater boundary is coincident with the top of the aquifer, whereas the present problem has an intervening aquitard between the seafloor and the aquifer. Also, they consider dispersive effects while this investigation intends to match the sharp interface assumed in Bakker's (2006) analytical solution. Kooi and Groen (2001) consider that aquifer salinization will arise when boundary layer theory predicts that the aquitard is entirely saline, but this neglects any boundary layer in the aquifer. In addition, validation is required to test the veracity of Kooi and Groen's (2001) method. Furthermore, in this analysis, the more physically realistic sea-floor boundary condition of different mass concentrations for inflow (seawater) and outflow (ambient groundwater) is adopted, whereas Kooi and Groen (2001) and Smith and Turner (2001) used specified-concentration boundary conditions. The flow-dependent concentration boundary condition used here is more realistic relative to the Dirichlet condition of previous subsea aquifer investigations, as explained by Abarca et al. (2007) and Smith (2004). That is, specified-concentration boundaries lead to anomalous backward dispersion effects for outflowing groundwater where it differs in concentration to the boundary value. Smith (2004) finds significant differences between the two boundary condition types in terms of mixed-convective processes in his evaluation of seawater recirculation rates. In this study, the alternative Rayleigh formulations (Ra^* and Ra_δ) are tested for applicability within the current conceptual framework.

2.3 Numerical modelling

2.3.1. SEAWAT

Numerical modelling is used to assess the offshore extent of freshwater and seawater in both the aquifer and aquitard below sea, under conditions that allow for comparison with the

Bakker (2006) solution. SEAWAT version 4 (Langevin et al., 2008) was adopted for this purpose. SEAWAT has been extensively tested and is widely used for the simulation of density-dependent groundwater flow and solute transport, combining MODFLOW-2000 (Harbaugh et al., 2000) and MT3DMS (Zheng and Wang, 1999). In general, SEAWAT solves in a coupled way, by a finite-difference method. The flow and transport components are coupled through the fluid density term, which is taken as a linear function of solute concentration. In general, the coupling of the flow equation and solute-transport equation consists of calculating fluid densities with the corresponding solute concentration from the previous timestep. Then, the mass transport model uses the resulting flow to calculate the new solute concentration considering diffusion, dispersion and advection processes. This new concentration gives rise to a new density field which in turns is incorporated back to the groundwater flow model as a relative density-difference term (Guo and Langevin, 2002).

The groundwater flow equation solved by SEAWAT is based on the concept of freshwater head or equivalent freshwater head. That is, when saline water is simulated, the model uses the equivalent freshwater head as the dependent variable in the variable-density groundwater flow equation. In environments where fluid density varies spatially, the groundwater pressure at the point of measurement (in real life tends to be the screen of the well) depends on the groundwater density (Post et al., 2007). Therefore, a normalised groundwater density is used, and freshwater is widely preferred. This indicates that if the native saline water in the well is entirely replaced with freshwater, in order to obtain the same groundwater pressure at the screen level, the new level of water would be higher since more fresh water will be needed to equal the same weight of saline water (Guo and Langevin, 2002). This is because freshwater is lighter than saline water. That new level of water measured at the same arbitrary datum is called the equivalent freshwater head. The program makes this conversion internally.

The governing equation for variable-density groundwater flow in terms of freshwater heads is as follows (Guo and Langevin, 2002):

$$\frac{\partial}{\partial \alpha}\left[\rho K_{fx}\left(\frac{\partial h_f}{\partial x}+\frac{\rho-\rho_f}{\rho_f}\frac{\partial Z}{\partial x}\right)\right]+\frac{\partial}{\partial y}\left[\rho K_{fy}\left(\frac{\partial h_f}{\partial y}+\frac{\rho-\rho_f}{\rho_f}\frac{\partial Z}{\partial y}\right)\right]$$
$$+\frac{\partial}{\partial z}\left[\rho K_{fz}\left(\frac{\partial h_f}{\partial z}+\frac{\rho-\rho_f}{\rho_f}\frac{\partial Z}{\partial z}\right)\right]=\rho S_f\frac{\partial h_f}{\partial t}+\theta\frac{\partial \rho}{\partial C}\frac{\partial C}{\partial t}-\rho_s q_s \quad (8)$$

Where K_{fx}, K_{fy} and K_{fz} are the equivalent freshwater hydraulic conductivity [L T^{-1}], S_f is the equivalent freshwater specific storage [L^{-1}], t is time [T], θ is effective porosity [-], C is solute concentration [M L^{-3}], ρ_s is the density of water entering from a source or leaving from a sink [M L^{-3}], and q_s is the volumetric flow rate per unit volume representing sources and sinks [T^{-1}].

The governing equation for solute transport used in SEAWAT is given as (Guo and Langevin, 2002):

$$\partial\frac{(\theta C)}{\partial t}=\Delta\cdot(\theta D\cdot\Delta C)-\Delta\cdot(\theta v C)+q_s C_s \quad (9)$$

Where D is the hydrodynamic dispersion coefficient [L^2 T^{-1}], v is the linear pore water velocity [L T^{-1}], C_s is the solute concentration of water entering/leaving from sources and sinks [M L^{-3}].

2.3.2. Formulating SEAWAT's GHB parameters

Explicit and implicit representations of the subsea aquitard are tested in numerical experiments, because implicit representation offers significant computational savings and is therefore an attractive option for practical, field-scale problems. In the explicit approach, the aquitard is subdivided into 11 model layers. An overlying specified-head boundary condition represents the hydrostatic head of the sea, and groundwater discharges at the ambient concentration, whereas inflowing water has seawater salinity. Implicit representation of the subsea aquitard is at least theoretically possible through application of SEAWAT's General Head Boundary (GHB) package (Langevin et al., 2008). The implicit approach is appealing because it adopts a similar conductance-based representation of the subsea aquitard as described by Bakker (2006). That is, the GHB package simulates flow (Q_{GHB}) [L^3 T^{-1}] into or out of a cell as a function of the difference in the heads of the cell and an external sink/source (Harbaugh, 2005). In the present case, the latter is the sea. Solute concentrations accompanying inflow and outflow via the GHB package are dealt with in the Sink and Source Mixing (SSM) package of MT3DMS (Zheng and Wang, 1999). A schematic of the GHB package is given in Figure 2-4 and is discussed in more detail below.

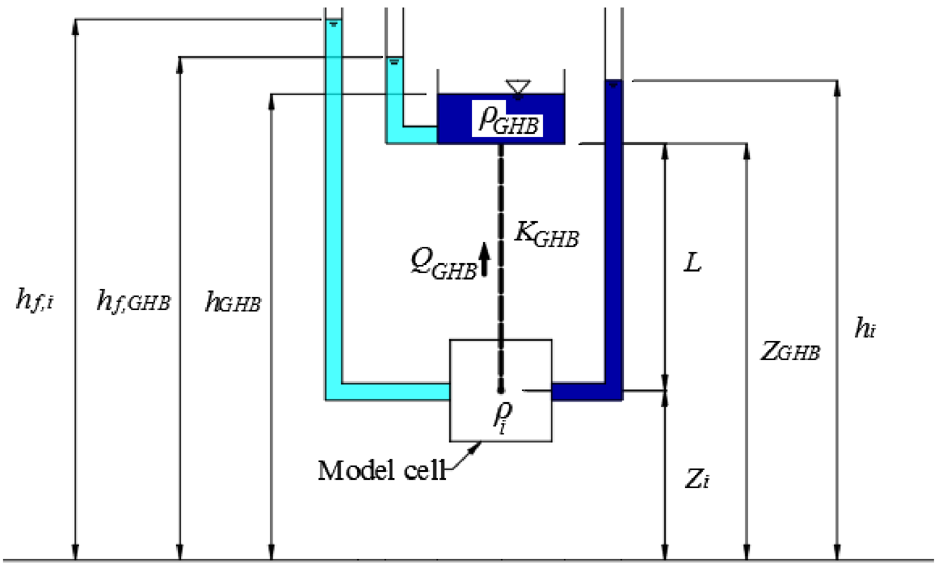

Figure 2-4. General conceptual model of the GHB package in SEAWAT. Light blue and dark blue 'manometers' show equivalent freshwater heads and heads respective of point water densities, respectively. Variables are described in the main body of the document.

The GHB package adopts the following formulation (Harbaugh, 2005):

$$Q_{GHB} = C\left[h_{f,i} - h_{f,GHB} + \frac{\overline{\rho} - \rho_f}{\rho_f}\left(Z_i - Z_{GHB}\right)\right] \quad (10)$$

Here, Z_i is the cell centre elevation, Z_{GHB} is the user-specified base elevation of the GHB reservoir, $h_{f,i}$ is the equivalent freshwater head at the centre of the model cell [L], and $h_{f,GHB}$ is the equivalent freshwater head at the base of the GHB reservoir (see Figure 2-4). SEAWAT obtains $h_{f,GHB}$ from the user-specified h_{GHB} (the water level in the GHB reservoir) using the formulation $h_{f,GHB} = h_{GHB}\left(\rho_{GHB}/\rho_f\right) - Z_{GHB}\left(\rho_{GHB} - \rho_f\right)/\rho_f$. SEAWAT determines the value of ρ_{GHB} through conversion of the user-specified solute concentration for the water in the GHB reservoir (seawater in this case). C is the user-specified boundary conductance [L^2 T^{-1}], given by $K_{GHB}A/L$, where K_{GHB} is the hydraulic conductivity between the GHB reservoir and the model cell [L T^{-1}], A is the area perpendicular to GHB flow [L^2], and L is the distance between the cell centre and the base of the GHB reservoir. $\overline{\rho}$ [M L^{-3}] represents the density of water between the GHB reservoir and the model cell.

SEAWAT's formulation of $\overline{\rho}$ makes application of the GHB package to the variable-density arrangement of Figure 2-4 challenging. $\overline{\rho}$ is assumed in SEAWAT to be constant, equal to the average of ρ_{GHB} and the fluid density of the model cell (ρ_i), whereas in reality, groundwater between the model cell and the boundary (i.e., in the aquitard) is likely to change depending on the direction of flow. SEAWAT's approach represents a simplification of otherwise unknown salinity conditions that occur within the aquitard (i.e., in the connection between the GHB reservoir and the boundary cell).

The most appropriate value of $\overline{\rho}$ for the simulation of subsea aquitards is presently unclear. To address this, a guidance is developed on the selection of GHB parameters for the current problem through model testing using various GHB parameter combinations. The intent is to apply the GHB package so that it reproduces, as closely as possible, the mathematics representing boundary discharge as adopted by Bakker (2006). Table 1 contains the final list of GHB parameters, given in terms of variables defined by Bakker (2006), and that reproduced Bakker's (2006) formulae for flow through the aquitard.

Table 1. GHB parameters defined in terms of variables relevant to Bakker's (2006) conceptual model.

GHB parameter	Bakker (2006) variable
Q_{GHB}	$q_z A$
A	$\Delta x^{\#}$
$L(=Z_{GHB}-Z_i)$	H_l
$C=(K_{GHB}/L)\,A$	$(K_z/H_l)\,A$
ρ_{GHB}^{*}	ρ_f
h_{GHB}	h_s
$h_{f,GHB}$	h_s
$h_{f,i}$	H

$^{\#}\Delta x$ is the cell width (assumes unit cell width perpendicular to the cross section)

$^{*}\rho_{GHB}$ is assigned a value of ρ_f, so that $h_{f,GHB} = h_{GHB}$ (see Figure 2-4)

By adopting H_l for L, we presume that the cell contains freshwater, thereby allowing L to be taken from the top of the cell (i.e., rather than from the cell centre, as shown in Figure 2-4) on the basis of the Dupuit assumption and because freshwater within the cell precludes the need to correct the cell's equivalent freshwater head for the reference elevation. Also, by taking $\rho_{GHB} = \rho_f$, $\overline{\rho} = \rho_f$ when the aquifer cell contains freshwater, thereby eliminating the buoyancy term from equation (10). Making the Table 1 substitutions, equation (10) reduces to equation (4), thereby replicating Bakker's (2006) formula.

Equation (10) arrives at equation (4) using Table 1 substitutions only when the subsea aquifer contains freshwater. However, the substitution of Table 1 parameters into equation (10) results in flow across the aquitard where the aquifer contains seawater (as apparent in the analysis that follows), in violation of the assumptions of Bakker (2006). To account for this, a modification is made to Table 1 parameter substitutions so that no flow will occur when the model cell contains seawater. That is, we require $Q_{GHB} = 0$ where $\rho_i = \rho_s$. Model cells representing the aquifer that are filled with seawater should reflect the hydrostatic head of the sea, giving rise to $h_{f,i} = Z_i + (z_s - Z_i)\rho_s/\rho_f$ (from direct application of Bernoulli's equation). Substituting these conditions into equation (10), considering the abovementioned definition of $\overline{\rho}$, and adopting a selection of the Table 1 substitutions, leads to:

$$0 = C\left[Z_i + \frac{\rho_s}{\rho_f}\left(z_s - Z_i\right) - h_s + \frac{\rho_s - \rho_f}{2\rho_f}\left(Z_i - Z_{GHB}\right)\right] \quad (11)$$

In equation (11), only Z_{GHB} can be adjusted without changing the freshwater flow formulation, because the buoyancy term is eliminated under freshwater conditions in the aquifer (as explained above). Thus, equation (11) is rearranged in terms of Z_{GHB}:

$$Z_{GHB} = \frac{2}{\rho_s - \rho_f}\left(\rho_s z_s - \rho_f h_s\right) - Z_i \quad (12)$$

Hence, in combination with the use of ρ_f for ρ_{GHB}, equation (12) creates vertical aquitard flow (at rates that assume that the aquitard contains seawater) where there is freshwater in the aquifer (following Bakker's (2006) approach), whereas there is no flow in the aquitard where the underlying aquifer contains only seawater.

An alternative GHB parameterisation is needed to represent the same conditions except where the aquitard contains freshwater where freshwater occurs in the underlying aquifer. For this case, the buoyancy term in equation (2) is removed, and the value for $h_{f,GHB}$ used in equation (10) is h_t. Again, we require Q_{GHB} = 0 where ρ_i = ρ_s, leading to the following substitution for Z_{GHB}:

$$Z_{GHB} = \frac{2}{\rho_s - \rho_f}\left(\rho_s z_s - \rho_f h_t\right) - Z_i \quad (13)$$

The approaches to GHB parameterisation described above were tested by comparing models that adopt implicit and explicit representations of the subsea aquitard.

2.3.3. Description of numerical experiments

Table 2 describes the baseline parameters used in the analytical and numerical models. Parameters are typical of previous coastal aquifer modelling by Kooi and Groen (2001), Post and Kooi (2003), Werner and Simmons (2009), Laattoe et al. (2013), and Werner (2017), with some trial and error to achieve tip positions that were landward of the model's seaward boundary. This was done to ensure that the tip position was sensitive to differences between models rather than located at the continental shelf. Two different scales were considered, labelled as Sections 1 and 2 in Table 2. The smaller domain size of Section 1 allowed for fine discretisation, and was used for cases of lower contrast between the aquitard K_z and the aquifer K. The longer extent of Section 2 provided insight into situations involving higher K.

Table 2. Parameters adopted in numerical and analytical models.

Parameter	Symbol	Section 1	Section 2	Unit
Onshore aquifer length	L_c	100.05	490	M
Offshore aquifer length	L_s	20	3000	M
Depth of the sea above the aquitard	H_s	20	20	M
Aquitard thickness	H_l	1	1	M
Aquifer depth	H	10	10	M
Hydrostatic seawater head	z_s	31	31	M
Aquifer hydraulic conductivity	K	10	10	m/d
Specific storage	S_s	10^{-5}	10^{-5}	1/m
Effective porosity	n	0.3	0.3	-
Freshwater density	ρ_f	1000	1000	kg/m^3
Seawater density	ρ_s	1025	1025	kg/m^3
Onshore head	h_o	32	32	M

Three phases of numerical experimentation were used to achieve the objectives of the investigation. In Phase 1, numerical models adopt an explicit representation of the offshore aquitard, allowing for physically based simulation of the mixed-convective processes occurring in the aquifer-aquitard system. Dispersion parameters were set to zero to reflect the sharp-interface approach of Bakker (2006), and only unavoidable artificial numerical dispersion creates widening of the mixing zone (Werner, 2017). The modelling results were compared to Bakker's (2006) solution to assess the validity of his underlying assumptions regarding the aquitard salinity. Phase 2 numerical modelling involves implicit representation of the offshore aquitard, commensurate with the approach of Bakker (2006), thereby exploring the use of the GHB package of SEAWAT in simulating offshore conditions. Substitutions as described in Section 2.3.2 were adopted to allow for different aquitard salinities to be tested and comparisons were made with models that simulate the aquitard explicitly. In Phase 3, dispersive effects were investigated, albeit briefly, through the addition of dispersive parameters of $D_m = 8.65 \times 10^{-5}$ m^2/d, α_L = 1 m, and transverse dispersivity (α_T) = 0.1 m, to the explicit model. In all three phases, several values of the aquifer K-aquitard K_z contrast were tested, as outlined in Table 3, which lists the parameters that differentiate the various numerical experiments.

Table 3. Description of numerical models for each modelling phase with the corresponding hydraulic conductivity values (aquifer *K* and aquitard K_z).

Phase	Model	Section	Onshore boundary freshwater inflow (Q_c)*	Aquitard K_z	Aquifer K: Aquitard K_z
			m^2/d	m/d	-
1	1	1	0.3480	5	2:1
	2	1	0.3417	1	10:1
	3	1	0.3361	0.5	20:1
	4	2	0.0675	0.01	1000:1
	5	2	0.0540	0.001	10000:1
	6	2	0.0308	0.0001	100000:1
2	7	1	0.3462	5	2:1
	8	1	0.3384	1	10:1
	9	1	0.3320	0.5	20:1
	10	1	0.3489	5	2:1
	11	1	0.3416	1	10:1
	12	1	0.3359	0.5	20:1
	13	2	0.0539	0.001	10000:1
	14	1	0.3469	5	2:1
	15	1	0.3400	1	10:1
	16	1	0.3340	0.5	20:1
3	1_d	1	0.3555	5	2:1
	2_d	1	0.3495	1	10:1
	3_d	1	0.3416	0.5	20:1

*Assuming unit cell size perpendicular to the cross section

Three different finite-difference grids were used, as shown in Figure 2-5. Models 1, 2, 3, 1_d, 2_d and 3_d adopted the model-domain grid shown in Figure 2-5(a), for which the horizontal resolution varies from 0.10 m at the seaward boundary increasing to 10 m at the landward boundary. The grid was designed such that the interface was contained within the part of the model with 0.10-m resolution. Layers are 0.10 m deep. The grid illustrated in Figure 2-5(b) was used for all implicit-aquitard models in Phase 2, and the grid resolution is the same as in Figure 2-5(a). Figure 2-5(c) represents the finite-difference grid used for Models 4, 5 and 6, for which the grid resolution represents a trade-off between model execution times and accuracy. The horizontal resolution varies from 50 m at the left-hand boundary decreasing to

2 m at the seaward boundary. The region of the model containing the interface has a 5-m horizontal discretisation. Vertical discretisation is again 0.10 m.

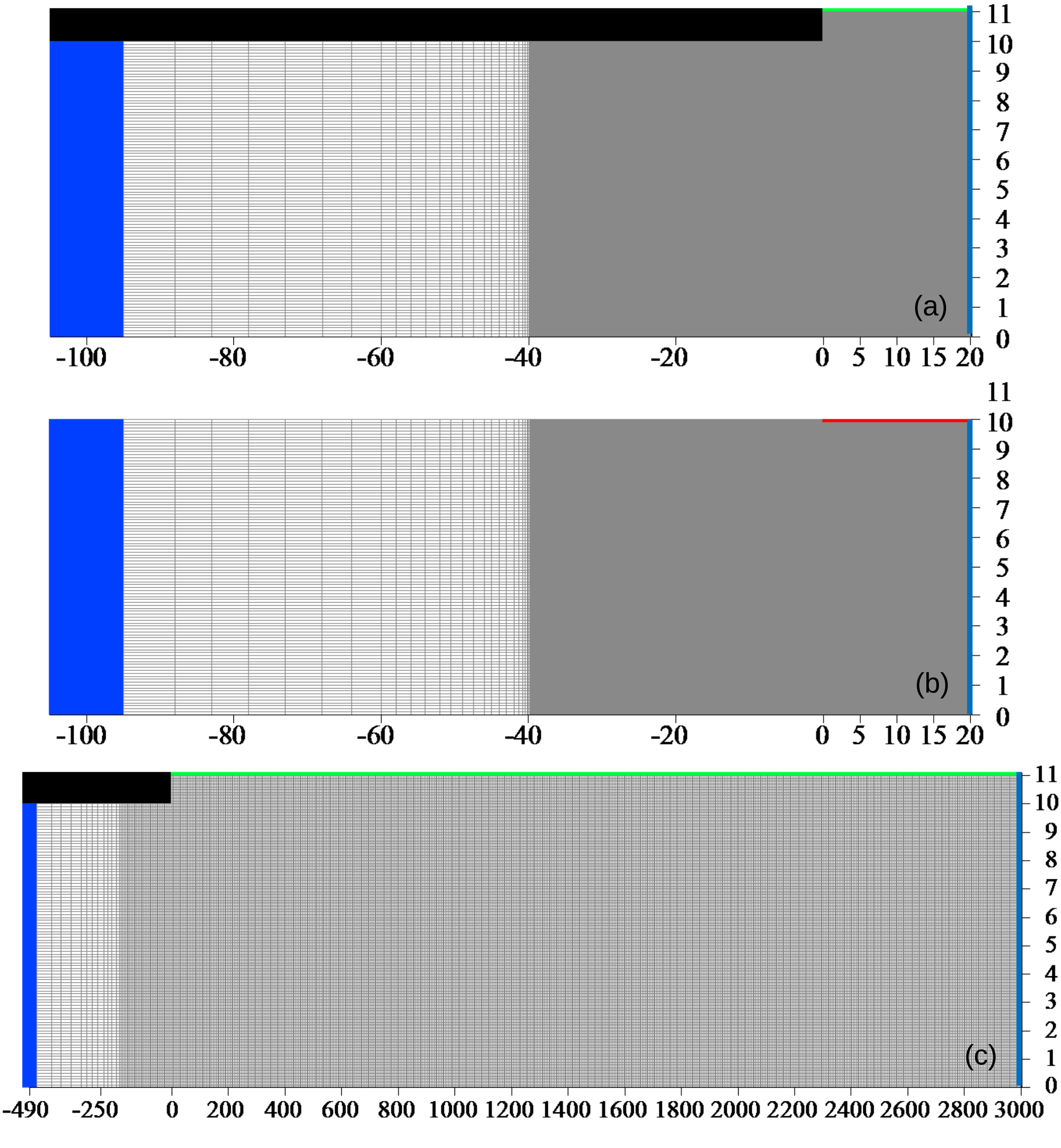

Figure 2-5. Finite-difference model grids used in this study. Blue cells at the landward freshwater boundary (left; relative solute concentration = 0) and at the seaward boundary (right; relative solute concentration = 1) represent specified-head conditions. Light green cells at the top of the model (Figures 2-5(a) and 2-5(b)) represent specified-head and flow-dependent concentration conditions using the CHD package (Langevin et al., 2008) to avoid issues of back dispersion identified by Abarca et al. (2007). Black regions are inactive cells. Red cells (top right of Figure 2-5(b)) show where the GHB package simulates flow through the aquitard. Horizontal distance is from the shoreline, and units are meters.

Three different salinity conditions were assigned to the aquitard in the Phase 2 numerical experiments. Models 7, 8 and 9 represent Bakker's (2006) assumption of seawater in the aquitard, while Models 10, 11, 12 and 13 presume that the aquitard contains freshwater (see Section 2.3.2 for GHB parameters). Finally, the default calculation of mixed water was tested, whereby the aquitard's water has a density equal to the average of freshwater and seawater. In this case, the program is used in its more "intuitive" form, whereby $h_{f,GHB}$ is calculated internally, and both ρ_{GHB} and Z_{GHB} represent the physical conditions, i.e., the seawater density and the equivalent freshwater head at the top of the aquitard, respectively. Table 4 summarises the case-specific parameters used in Phase 2.

Table 4. Specified parameter values into the GHB package for Phase 2.

Model	Specified water head at the GHB reservoir		Elevation at the base of the GHB reservoir Z_{GHB}	SEAWAT conductance C	Solute concentration of the GHB reservoir
	$h_{f,GHB}$	h_{GHB}			
	m	m	m	m^2/d	kg/m^3
7	31.525		10.05*	0.50	0
8	31.525		10.05	0.10	0
9	31.525		10.05	0.05	0
10	31.500		12.05**	0.50	0
11	31.500		12.05	0.10	0
12	31.500		12.05	0.05	0
13	31.500		12.05	0.005	0
14		31	11	0.50	35
15		31	11	0.10	35
16		31	11	0.05	35

*Value of ZGHB calculated with equation (12).
**Value of ZGHB calculated with equation (13).

3. Results

3.1 Phase 1

Figure 3-1 shows the steady-state salinity distributions for the six models of Phase 1, compared to Bakker's (2006) analytical solution. The 0.5 isochlor is adopted as representative of the transition between freshwater and seawater, because this concentration is widely used to indicate the penetration of seawater in variable-density problems (e.g., Abarca et al., 200; Sebben et al., 2015). Significant differences between the numerical results and Bakker's (2006) analytical solution are found in the offshore distance to the interface tip (x_{tip}). For example, the analytical solution estimates that x_{tip} reaches the end of the offshore aquifer in Model 3, whereas the numerical model predicts that the freshwater body reaches only the midpoint of the offshore aquifer. Aside from the discrepancy in x_{tip}, the analytical solution provides a reasonable match to most of the interfaces' shapes. Calculations of the interface toe position (x_{toe}) are in close agreement.

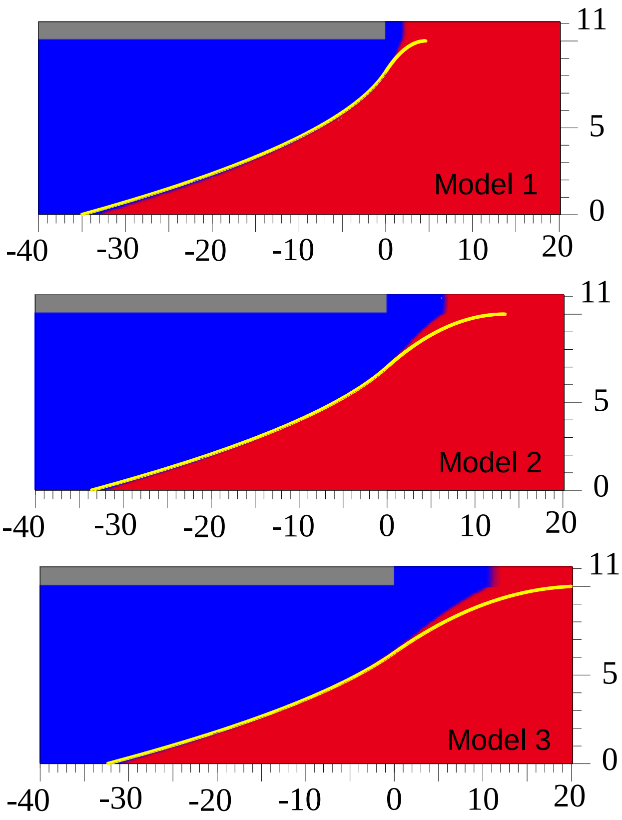

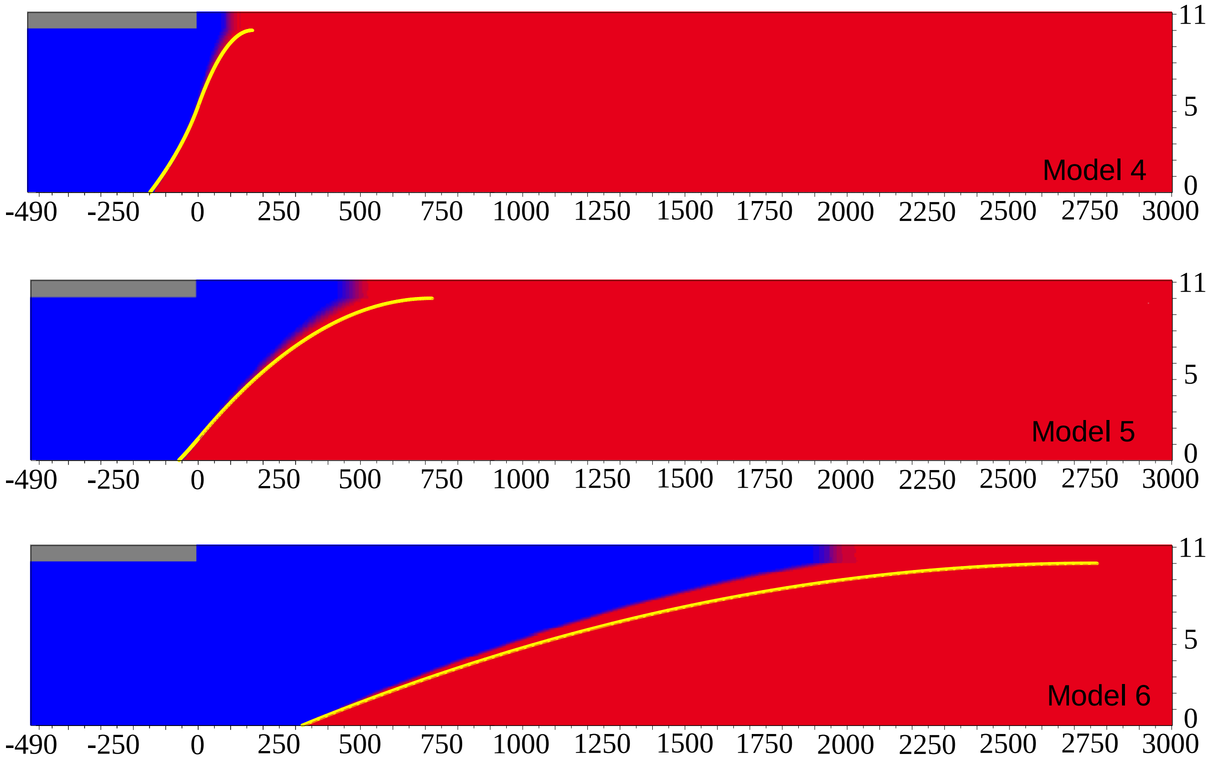

Figure 3-1. Comparison between numerical model salinity distributions (colour distribution, where blue is freshwater and red is seawater) and Bakker's (2006) sharp-interface location (yellow line) from Phase 1 models. The 0.5 isochlor is adopted as representative of the transition between freshwater and seawater. Horizontal distance is from the shoreline. Units are metres. Model geometry and description of cases are given in Table 2 and 3. Only the first inland 40 m are depicted for Models 1 to 3, to highlight the mixing zone characteristics.

A quantitative comparison between numerical and analytical results from Phase 1 is given in Figure 3-2, in which the 0.5 isochlor has been used to represent x_{tip} in numerical results. Figure 3-2 shows that x_{tip} over-prediction is greater in situations where the aquifer *K*-aquitard K_z contrast is smaller. The discrepancy ranges between 41% (high contrast) and 142 % (low contrast).

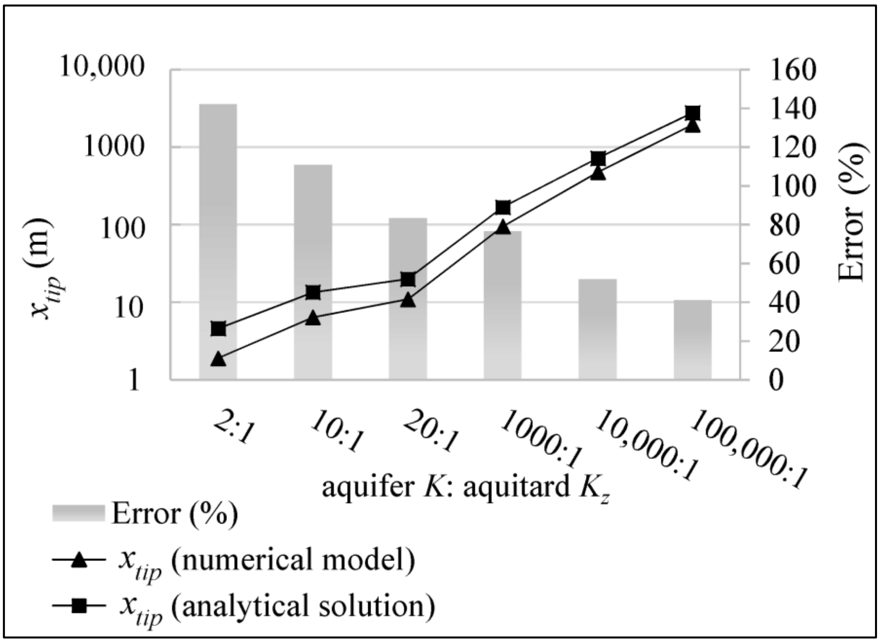

Figure 3-2. Comparison of analytically and numerically derived x_{tip} for Phase 1 models. Errors are calculated as: 100×(analytical x_{tip} – numerical x_{tip})/numerical x_{tip}.

The Darcy velocities depicted in Figure 3-3 show the flow patterns in the aquitard produced by SEAWAT. Figure 3-3 also shows an enlarged representation of the mixing zone within the aquitard, which widens as K_z is reduced (for a given aquifer K). This is consistent with observations by Lu et al. (2013), who undertook sand-tank and numerical experiments of interface behaviour in stratified aquifers. The location of the divide between upwards and downwards flow in the aquitard (Figure 3-3) occurs where the salinity is between the 0.9 and 0.99 isochlor. Here, salinity is represented as relative to seawater. Thus, there is significant upward flow of seawater within the mixing zone, whereas analytical methods account for the upward flow of only freshwater. Huyakorn et al. (1987) obtained a similar outcome from numerical modelling of seawater intrusion in a semi-confined, sub-sea aquifer, in which upward flow of groundwater with salinities greater than the 0.9 isochlor occurred. The recirculation of seawater in classical homogeneous coastal aquifer situations is well known (e.g. Smith, 2004), and is driven by mixed-convection processes that lead to “convective overturn” of the seawater body.

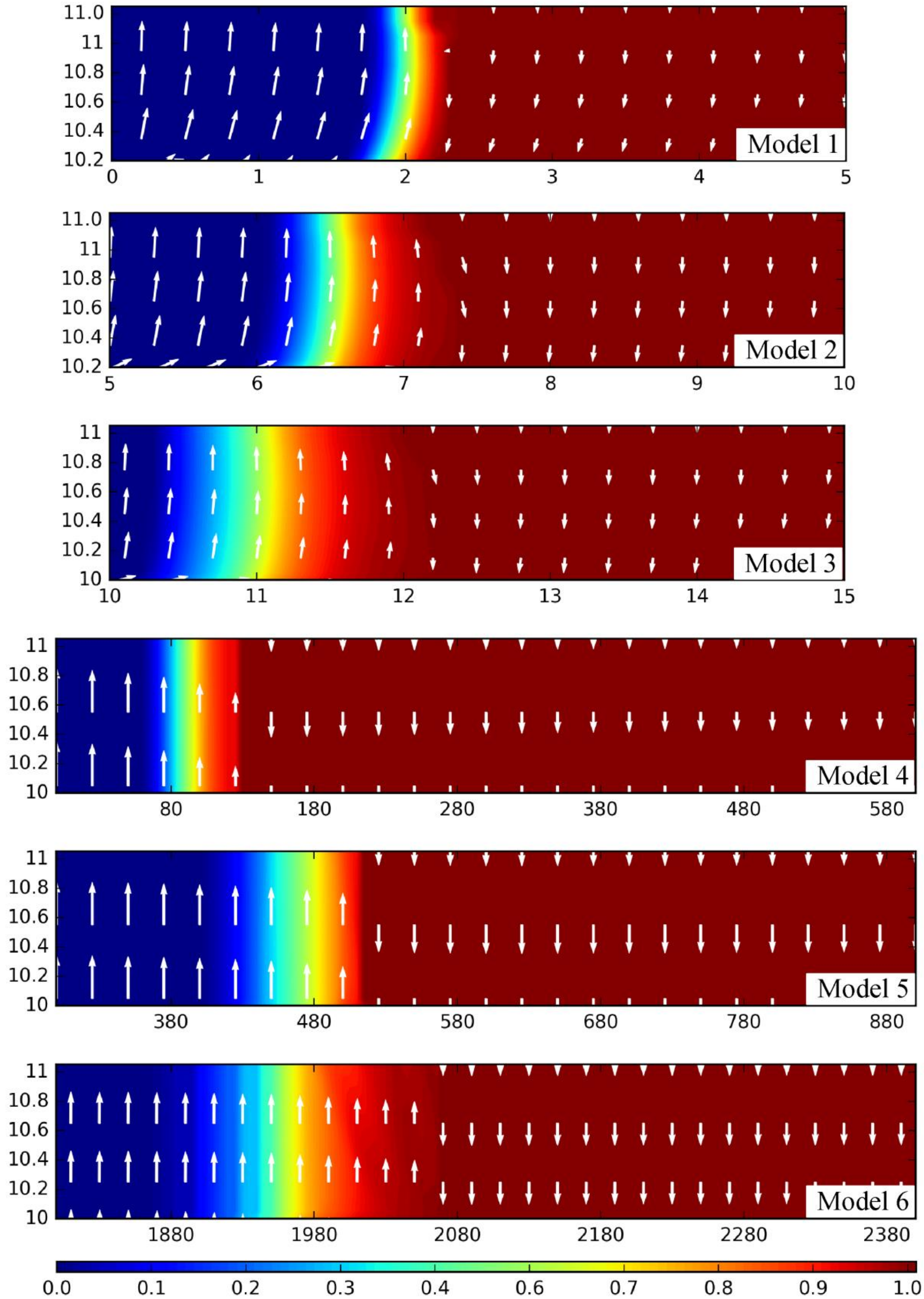

Figure 3-3. Velocity vectors and salinity contours within the aquitard for Models 1 to 6. Arrow size follows a logarithmic relationship with velocity magnitude. Distances are from the shoreline. The horizontal scale differs between models. Units are meters. Contours: relative to seawater salinity.

The occurrence of downward flow (Figure 3-3) implies that buoyancy forces have overcome advective forces associated with SFGD, and therefore, downward flow is expected to occur at high Rayleigh numbers. However, Ra_c values are drawn from the salinity distribution rather than from velocities, because the Rayleigh theory applied to mixed-convective problems is based on the occurrence of density-driven convective flow in situations where the flow is upwards (e.g., Wooding et al., 1997). The Rayleigh number of Wooding et al. (1997), Ra_δ, given as equations (6) was obtained from the Phase 1 modelling results. The upward flow at the base of the aquitard was used for the calculation of δ (equation (5)). Figure 3-4 shows the values of Ra_δ for three different salinity conditions: 0.1 isochlor, 0.5 isochlor and 0.9 isochlor. The 0.5 isochlor is adopted as representative of the transition between advection-dominated and buoyancy-dominated conditions in the aquitard. The value of Raδ for the 0.5 isochlor seen in Figure 3-4 is relatively consistent across the six models, at approximately two, whereas there is variation in Raδ for the 0.1 and 0.9 isochlors.

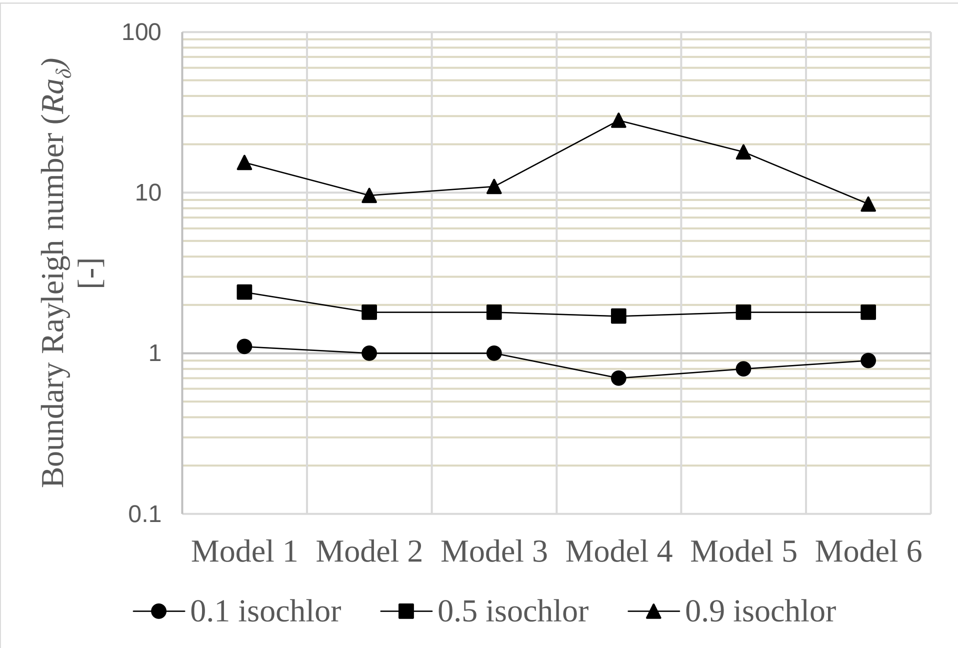

Figure 3-4. Ra_δ values for the 0.1 isochlor, 0.5 isochlor, and 0.9 isochlor in Phase 1 modelling results.

3.2 Phase 2

Figure 3-5 shows the steady-state salinity distribution when the aquitard is implicitly simulated presuming seawater in it, compared to Bakker's (2006) analytical solution. The results show that the numerical simulations are in good agreement with the analytical solution. These results confirm the parameterisation of the GHB package, aimed at reproducing Bakker's (2006) assumptions, that was developed in Section 2.3.2. The comparisons shown in Figure 3-5 validate that the implicit method can be used (with confidence) to explore other assumed values for salinity within the aquitard.

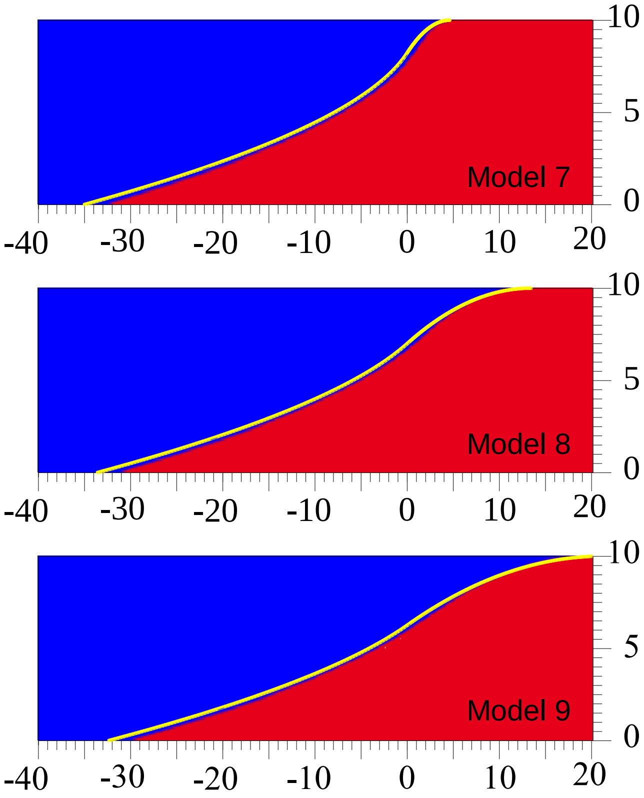

Figure 3-5. Numerical simulations for Phase 2 when seawater is contained in the aquitard (colour distribution, where blue is freshwater and red is seawater) and Bakker's (2006) sharp interface location (yellow line). Horizontal distance is from the shoreline. Units are meters. Model geometry and description of cases are given in Table 2 and 3. Only the first inland 40 m are depicted to highlight the mixing zone characteristics.

Figure 3-6 illustrates salinity distributions obtained when the aquitard, represented implicitly in numerical models, is presumed to contain freshwater. These are compared to Bakker's (2006) analytical solution. The results are also compared against the modelling results where the aquitard is simulated explicitly (shown by the black arrow in Figure 3-6, which indicates the tip of the 0.5 isochlor). An excellent match between the freshwater assumption in the implicit simulation of the aquitard and models simulating the aquitard explicitly is observed.

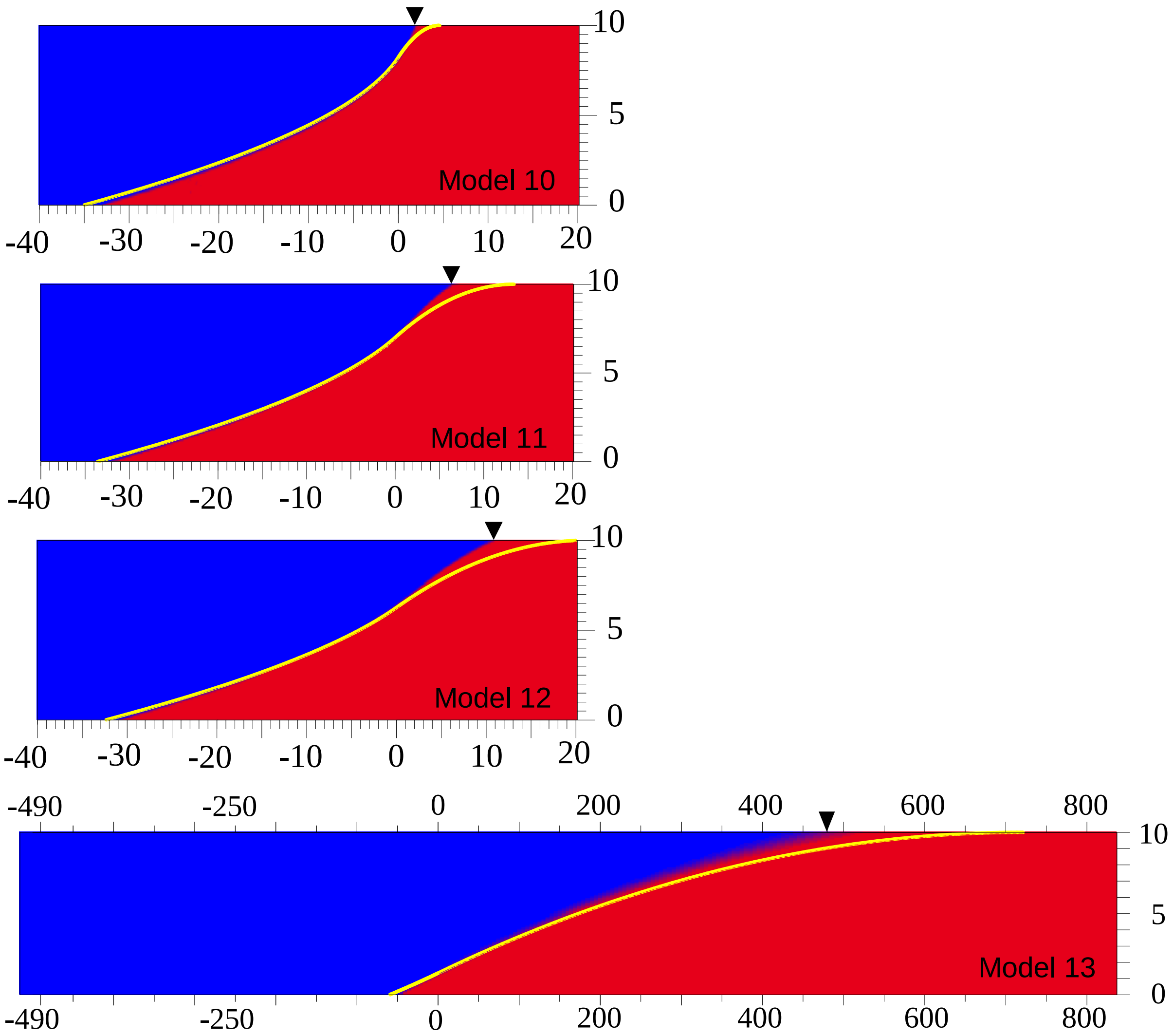

Figure 3-6. Numerical simulations for Phase 2 when freshwater is contained in the aquitard (colour distribution, where blue is freshwater and red is seawater) and Bakker's (2006) sharp interface location (yellow line). Horizontal distance is from the shoreline. Units are meters. Model geometry and description of cases are given in Table 2 and 3. In Models 10, 11 and 12 only the first inland 40 m are depicted, and in Model 13, the first 800 m offshore are depicted to highlight the mixing zone characteristics. Black arrow shows the resulting tip position in the corresponding explicit numerical model (i.e., Phase 1) for the 0.5 isochlor.

Finally, Figure 3-7 shows the simulation results of models 14, 15 and 16, that is, when the option of mixed water is assumed as it is internally used in the GHB package. In this case, the results show relatively poor agreement between the numerical and analytical solution as compared with the results of assuming freshwater within the aquitard (shown by the black arrow in Figure 3-7, which indicates the tip of the 0.5 isochlor).

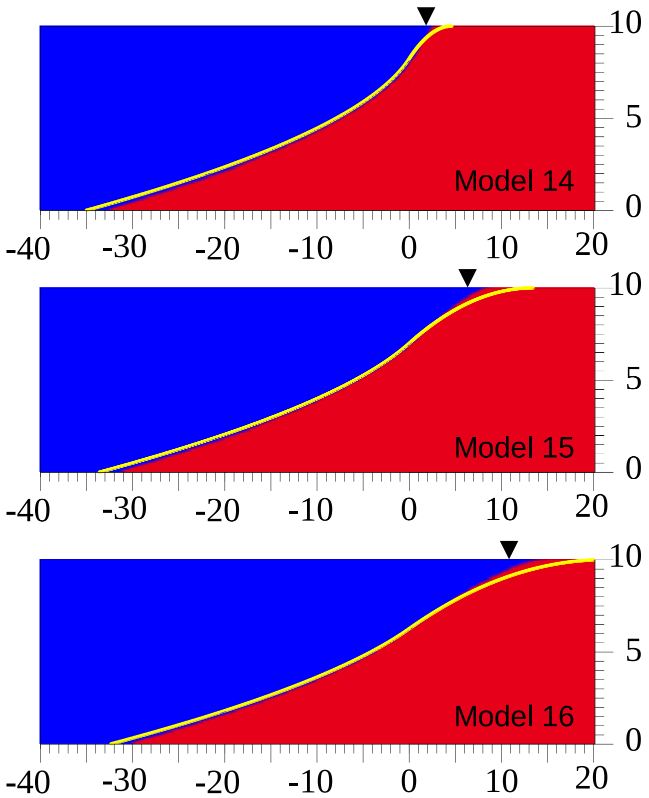

Figure 3-7. Numerical simulations for Phase 2 when mixed water is contained in the aquitard (colour distribution, where blue is freshwater and red is seawater) and Bakker's (2006) sharp interface location (yellow line). Horizontal distance is from the shoreline. Units are meters. Model geometry and description of cases are given in Table 2 and 3. Only the first inland 40 m are depicted to highlight the mixing zone characteristics. Black arrow shows the resulting tip position in the corresponding explicit numerical model (i.e., Phase 1) for the 0.5 isochlor.

3.3 Phase 3

Figure 3-8 shows the effects of dispersion on the salinity distribution for the conceptual conditions of this study. Compared to the corresponding thin mixing zone simulations (see Figure 3-1), the extent of seawater is reduced. Particularly, the toe position is located farther offshore. However, the offshore distance of the outflow face through the aquitard, taken at the 0.5 isochlor, is less sensitive to the dispersion process.

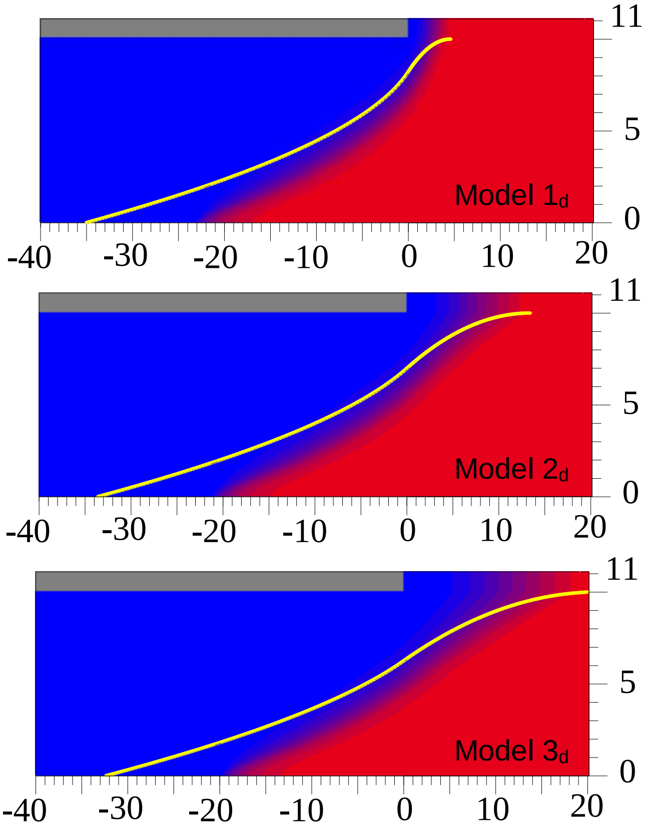

Figure 3-8. Comparison between numerical model salinity distributions (colour distribution, where blue is freshwater and red is seawater) and Bakker's (2006) sharp-interface location (yellow line) from Phase 3 models. The 0.5 isochlor is adopted as representative of the transition between freshwater and seawater. Horizontal distance is from the shoreline. Units are meters. Model geometry and description of cases are given in Table 2 and 3. Only the first inland 40 m are depicted for Models 1_d to 3_d, to highlight the mixing zone characteristics.

To calculate the Rayleigh number of Smith and Turner (2001), Ra^*, given as equation (7), the models' results of Phase 3 were used. The total length of upward flow at the base of the aquitard with salinity up to the 0.5 isochlor was used to calculate U_d in equation (7). Figure 3-9 shows the Ra^* calculated for Models 1_d, 2_d and 3_d.

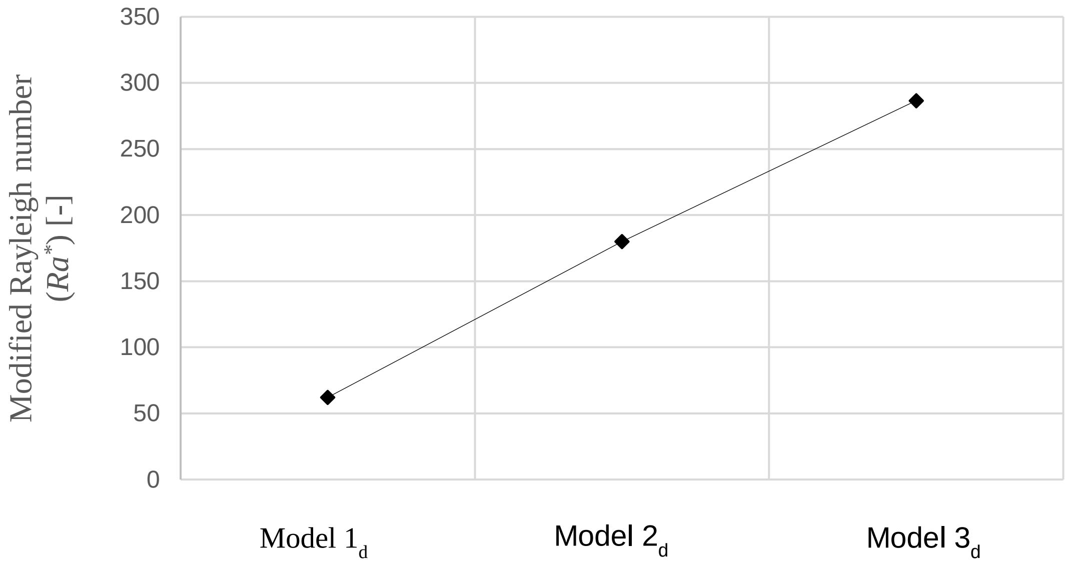

Figure 3-9. Ra_δ values for the 0.5 isochlor.

4. Discussion

The Phase 1 results show that the analytical solution tends to overpredict x_{tip}. The results also show that x_{tip} increases as the aquitard K_z is reduced for a constant aquifer K showing agreement with the reports of Frind (1982). Also, the mixing zone in the aquitard widens when the aquitard K_z is reduced (Figure 3-3), consistent with numerical modelling and sand-tank experiments of stratified aquifers by Lu et al. (2013). According to Lu et al. (2013), upward diluted seawater is refracted when flowing from a higher-K unit (aquifer) towards an overlying lower-K layer (aquitard) producing separation of streamlines within the aquitard, which in turn enhances the width of the mixing zone. This phenomenon may contribute to the smaller (but nonetheless significant) discrepancy between Phase 1 numerical models and Bakker's (2006) analytical solution as the aquifer K-aquitard K_z contrast increases (see Figure 3-2). That is, enhanced mixing in the aquitard under strong K contrasts may lead to higher solute concentrations in the aquitard, which tends towards the assumption by Bakker (2006) that the aquitard contains seawater.

Seawater recirculation and other dispersive effects in the results of this study are caused by unavoidable artificial dispersion (e.g., Werner, 2017). Artificial dispersion appears to have only a small influence on the interface location, given the close correlation between numerical and analytical methods observed in Phase 2 (i.e., Figure 3-5). Nevertheless, artificial dispersion allows for a Rayleigh-type analysis of the mixed-convective processes occurring in the aquitard. The Ra_δ value of approximately two, which corresponds to the occurrence of the 0.5 isochlor in all models, is therefore the Ra_c at which the convective circulation is the dominant force.

The effect of dispersion was briefly assessed in Phase 3. The reduction of seawater extent, when compared with the corresponding sharp-interface models (see Figure 3-1) is due to the fact that the toe position is located farther offshore (e.g., Cooper, 1959), whereas the tip position is less affected. However, the dispersion parameter chosen for this analysis is large (i.e., α_L=1 m) with respect to the thickness of the aquitard (i.e., H_l=1 m). Therefore, a lower value should be tested that conforms with the grid Péclet number constraint (e.g., Lu et al., 2013).

The GHB package was effective in reproducing Bakker's (2006) analytical solution (Figure 3-5) subject to adjustments in specified parameters that do not represent the physical characteristics of the conceptual model. That is, using equations (12) and (13) to adjust the value of Z_{GHB}. Also, the application of the GHB package has helped to suggest that the resulting overestimation in Bakker's (2006) analytical solution is associated to the salinity assumption in the aquitard. Figure 3-6 shows that the explicit modelling results (i.e., black arrow in Figure 3-6) are in agreement with Models 10, 11, 12 and 13.

Finally, in Figure 3-7 is observed that when the default application of the GHB package is used, that is when mixed water is assumed to be contained in the aquitard, the offshore extension of freshwater is overestimated. Results show that this deviation ranges between 30-50%, decreasing as the aquifer K-aquitard K_z contrast rises.

5. Conclusions

This study has employed both explicit and implicit representations of the subsea aquitard to assess the offshore extent of freshwater and seawater in submarine aquifers predicted by the analytical solution of Bakker (2006). The explicit approach whereby the aquitard was discretised into 11 layers is the more physically reliable approach used to evaluate the analytical solution and the implicit models' results. The interest in using the GHB application as an implicit approach relied on the similar mathematical formulation shared with the analytical solution. In this study, the assessment of the assumption of seawater within the aquitard has been an integral part of the analysis. The major findings are as follows:

1) Bakker's (2006) analytical solution tends to overpredict the offshore extension of the freshwater outflow face under the subsea aquitard, whereas the calculation of the toe position of the seawater wedge is fairly well predicted. Despite the overestimation of the freshwater extent is reduced as the aquifer K-aquitard K_z contrast is increased, for the largest contrast analysed in this study (i.e.,100000:1) the obtained error (i.e., ≈41%) is still significant. In this study, the K in the aquifer was remained constant and only K_z values in the aquitard were changed to simulate the contrast.

2) The truncation of SFGD (based on the 0.5 isochlor) can be satisfactorily predicted through the Rayleigh theory. The Ra_δ proposed by Wooding et al. (1997), applying the δ estimation proposed by Kooi and Groen (2001) provided consistent values for the six models of the explicit approach. In this study, $Ra_\delta \approx 2$ indicates the critical value to estimate the truncation of freshening upward flow through the aquitard. It is difficult to apply the Ra^* suggested by Smith and Turner (2001) as no congruency was found between the three models simulated for Phase 3.

3) The GHB package was effective in reproducing Bakker's (2006) analytical solution (Figure 3-5) and therefore, it was possible to test different salinity conditions within the aquitard. However, the GHB application as an alternative to the explicit representation of the subsea aquitard has some limitations. On one hand, when the physical and geometric parameters that directly describe the conceptual model of Figure 2-1 are used, the GHB application calculates a mixed water in the aquitard that tends to overestimate the tip of the interface as it was seen in Models 14, 15 and 16. For the three models studied, this overestimation is approximately 30-50%. On the other hand, when the GHB approach is used to reproduce Bakker's (2006) analytical solution, adjustments in specified parameters that do not represent the real physical characteristics of the conceptual model must be employed. Specifically, adjustment of the user-specified Z_{GHB} parameter is needed by using equations (12) when it is considered that the aquitard contains seawater, and equation (13) when the alternative of freshwater is used.

4) The salinity distribution in the submarine aquifer predicted by Bakker's (2006) analytical solution is strongly influenced by the salinity assumption within the aquitard. The unrealistic saline condition in an aquitard accommodating SGFD was also commented by Kooi and Groen (2001) in the study of their analytical solution. Unfortunately, their proposal to correct this limitation (i.e., the δ-based truncation) provided no consistent agreement with their numerical modelling results. In this study, the impact of the saline aquitard condition has been evident in the attempt to reproduce Bakker's (2006) analytical solution when freshwater is considered to be contained within the aquitard. The results indicate that Bakker's (2006) analytical

solution, if the aquitard's salinity condition is considered fresh, provides the same results as those models simulating the aquitard explicitly. Therefore, it is proposed that the aquitard's salinity condition assumed in Bakker's (2006) analytical solution should be reconsidered. More specifically, it has been found that Bakker's (2006) analytical solution can be reliably applied to predict the extent of offshore freshwater if the assumption of salinity within the aquitard is changed towards freshwater. Numerically, this can be achieved using the GHB package by adjusting the Z_{GHB} parameter with equation (13).

6. References

Abarca, E, Carrera, J, Sánchez-Vila, X & Dentz, M 2007, 'Anisotropic dispersive Henry problem', *Advances in water resources*, vol. 30, no. 4, pp. 913-26.

Bakker, M 2006, 'Analytic solutions for interface flow in combined confined and semi-confined, coastal aquifers', *Advances in water resources*, vol. 29, no. 3, pp. 417-25.

Bakker, M, Miller, AD, Morgan, LK & Werner, AD 2017, 'Evaluation of analytic solutions for steady interface flow where the aquifer extends below the sea', *Journal of Hydrology*.

Cohen, D, Person, M, Wang, P, Gable, CW, Hutchinson, D, Marksamer, A, Dugan, B, Kooi, H, Groen, K & Lizarralde, D 2010, 'Origin and extent of fresh paleowaters on the Atlantic continental shelf, USA', *Ground Water*, vol. 48, no. 1, pp. 143-58.

Cooper, H 1959, 'A hypothesis concerning the dynamic balance of fresh water and salt water in a coastal aquifer', *Journal of Geophysical Research*, vol. 64, no. 4, pp. 461-7.

Edelman, J. H. 1972. Groundwater hydraulics of extensive aquifers. International Institute for Land Reclamation and Drainage Bulletin, vol. 13. Wageningen, The Netherlands (216 p.).

Frind, EO 1982, 'Seawater intrusion in continuous coastal aquifer-aquitard systems', *Advances in water resources*, vol. 5, no. 2, pp. 89-97.

Groen, J, Velstra, J & Meesters, AGCA 2000, 'Salinization processes in paleowaters in coastal sediments of Suriname: Evidence from δ37Cl analysis and diffusion modelling', *Journal of Hydrology*, vol. 234, no. 1-2, pp. 1-20.

Guo, W., Langevin, C. D. 2002. User's guide to SEAWAT: a computer program for simulation of three-dimensional variable-density ground-water flow. Technical Report, U.S. Geological Survey Techniques and Methods, Book 6, Chapter A7, 77 pp.

Harbaugh, A. W. (2005), MODFLOW-2005, the US Geological Survey modular ground-water model: The ground-water flow process, U.S. Geological Survey. Tech. Methods, 6-A16.

Harbaugh AW, Banta ER, Hill MC, McDonald MG (2000) MODFLOW-2000, the U.S. Geological Survey modular ground-water model—User guide to modularization concepts and the Ground-Water Flow Process: U.S. Geological Survey Open-File Report 00–92, 121 p.

Huyakorn, PS, Andersen, PF, Mercer, JW & White, HO 1987, 'Saltwater intrusion in aquifers: Development and testing of a three-dimensional finite element model', *Water Resources Research*, vol. 23, no. 2, pp. 293-312.

Jiao, JJ, Shi, L, Kuang, X, Lee, CM, Yim, WWS & Yang, S 2015, 'Reconstructed chloride concentration profiles below the seabed in Hong Kong (China) and their implications for offshore groundwater resources', *Hydrogeology Journal*, vol. 23, no. 2, pp. 277-86.

Johnston, RH 1983, 'The saltwater-freshwater interface in the Tertiary limestone aquifer, southeast Atlantic outer-continental shelf of the USA', *Journal of Hydrology*, vol. 61, no. 1-3, pp. 239-49.

Kooi, H & Groen, J 2001, 'Offshore continuation of coastal groundwater systems; predictions using sharp-interface approximations and variable-density flow modelling', *Journal of Hydrology*, vol. 246, no. 1, pp. 19-35.

Kwong, HT & Jiao, JJ 2016, 'Hydrochemical reactions and origin of offshore relatively fresh pore water from core samples in Hong Kong', *Journal of Hydrology*, vol. 537, pp. 283-96.

Langevin, C.D., Thorne Jr., D.T., Dausman, A.M., Sukop, M.C., Guo, W., 2008. SEAWAT version 4: a computer program for simulation of multi-species solute and heat transport: U.S. Geological Survey Techniques and Methods, Book 6, Chap. A22, 39 p, http://pubs.usgs.gov/tm/tm6a22/.

Laattoe, T, Werner, AD & Simmons, CT 2013, 'Seawater intrusion under current sea-level rise: processes accompanying coastline transgression', in Groundwater in the Coastal Zones of Asia-Pacific, Springer, pp. 295-313.

Lu, C, Chen, Y, Zhang, C & Luo, J 2013, 'Steady-state freshwater–seawater mixing zone in stratified coastal aquifers', *Journal of Hydrology*, vol. 505, pp. 24-34.

Marksamer, AJ, Person, MA, Day-Lewis, FD, Lane, JW, Cohen, D, Dugan, B, Kooi, H & Willett, M 2007, *Integrating geophysical, hydrochemical, and hydrologic data to understand the freshwater resources on Nantucket Island, Massachusetts*, Wiley Online Library.

Post, VE & Kooi, H 2003, 'Rates of salinization by free convection in high-permeability sediments: insights from numerical modeling and application to the Dutch coastal area', *Hydrogeology Journal*, vol. 11, no. 5, pp. 549-59.

Post, V, Kooi, H & Simmons, C 2007, 'Using hydraulic head measurements in variable-density ground water flow analyses', Groundwater, vol. 45, no. 6, pp. 664-71.

Post, VEA, Groen, J, Kooi, H, Person, M, Ge, S & Edmunds, WM 2013, 'Offshore fresh groundwater reserves as a global phenomenon', *Nature*, vol. 504, no. 7478, pp. 71-8.

Sebben, ML, Werner, AD & Graf, T 2015, 'Seawater intrusion in fractured coastal aquifers: A preliminary numerical investigation using a fractured Henry problem', *Advances in water resources*, vol. 85, pp. 93-108.

Simmons, CT, Bauer-Gottwein, P, Graf, T, Kinzelbach, W, Kooi, H, Li, L, Post, V, Prommer, H, Therrien, R, Voss, CI, Ward, J & Werner, A 2010, 'Variable density groundwater flow: From modelling to applications', in *Groundwater Modelling in Arid and Semi-Arid Areas*, pp. 87-118.

Smith, AJ 2004, 'Mixed convection and density-dependent seawater circulation in coastal aquifers', *Water Resources Research*, vol. 40, no. 8, pp. W083091-W0830916.

Smith, AJ & Turner, JV 2001, 'Density-dependent surface water–groundwater interaction and nutrient discharge in the Swan–Canning Estuary', *Hydrological Processes*, vol. 15, no. 13, pp. 2595-616.

Thomann, J. (2017), Investigating the extent and vulnerability of fresh groundwater beneath the sea: Application of sharp-interface analytical methods, Undergraduate thesis, 131 pp., Flinders University, Adelaide, South Australia.

Werner, AD 2017, 'On the classification of seawater intrusion', In press, *Journal of Hydrology*.

Werner, AD & Simmons, CT 2009, 'Impact of sea-level rise on sea water intrusion in coastal aquifers', *Ground Water*, vol. 47, no. 2, pp. 197-204.

Wooding, RA, Tyler, SW & White, I 1997, 'Convection in groundwater below an evaporating salt lake: 1. Onset of instability', *Water Resources Research*, vol. 33, no. 6, pp. 1199-217.

Zheng, C., Wang, P.P., 1999. MT3DMS: A modular three-dimensional multispecies transport model for simulation of advection, dispersion, and chemical reactions of contaminants in groundwater systems; documentation and user's guide. US Army Corps of Engineers Engineer Research and Development Center Contract Report SERDP-99-1.